Published in final edited form as:

Cancer Res. 2018 July 15; 78(14): 3865–3876. doi:10.1158/0008-5472.CAN-18-0056.

Osteocyte-Driven Downregulation of Snail Restrains Effects of Drd2 Inhibitors on Mammary Tumor Cells

Shengzhi Liu[1,2], **Yao Fan**[1,2], **Andy Chen**[2], **Aydin Jalali**[2], **Kazumasa Minami**[3], **Kazuhiko Ogawa**[3], **Harikrishna Nakshatri**[4], **Bai-Yan Li**[1], and **Hiroki Yokota**[1,2]

[1]Department of Pharmacology, School of Pharmacy, Harbin Medical University, Harbin 150081, China

[2]Department of Biomedical Engineering, Indiana University Purdue University Indianapolis, Indianapolis, IN 46202, USA

[3]Department of Radiation Oncology, Osaka University Graduate School of Medicine Suita, Osaka 565-0871, Japan

[4]Department of Surgery, Simon Cancer Research Center, Indiana University School of Medicine, Indianapolis, IN 46202, USA

Abstract

While bone is a frequent target of breast cancer-associated metastasis, little is known about the effects of tumor-bone interactions on the efficacy of tumor-suppressing agents. Here we examined the effect of two FDA-approved dopamine modulators, Fluphenazine (FP) and Trifluoperazine (TFP), on mammary tumor cells, osteoclasts, osteoblasts, and osteocytes. These agents suppressed proliferation and migration of mammary tumor cells chiefly by antagonizing dopamine receptor D2 and reduced bone resorption by downregulating nuclear factor of activated T-cells, cytoplasmic 1 (Nfatc1). Three-dimensional spheroid formation assays revealed that tumor cells have high affinity to osteocytes and type I collagen, and interactions with osteocytes as well as administration of FP and TFP downregulated Snail and suppressed migratory behaviors. Unlike the inhibitory action of FP and TFP on tumor growth, tumor-osteocyte interactions stimulated tumor proliferation by upregulating NFκB and Akt. In the bone microenvironment, osteocytes downregulated Snail and acted as an attractant as well as a stimulant to mammary tumor cells. These results demonstrate that tumor-osteocyte interactions strengthen dopamine receptor-mediated suppression of tumor migration but weaken its inhibition of tumor proliferation in the osteocyte-rich bone microenvironment.

Keywords

breast cancer; bone metastasis; dopaminergic signaling; osteocytes; *Snail*

Co-corresponding Authors: Hiroki Yokota, PhD, Department of Biomedical Engineering, Indiana University-Purdue University Indianapolis, 723 West Michigan Street, SL220, Indianapolis, IN 46202 USA, Phone: 317-278-5177; Fax: 317-278-2455, hyokota@iupui.edu; Bai-Yan Li, MD/PhD, Department of Pharmacology, School of Pharmacy, Harbin Medical University, 157 Baojian Road, Harbin 150081, China, Phone/Fax: +86 451-8667-134, liby@ems.hrbmu.edu.cn.

Competing interests: The authors declare no conflict of interest.

Introduction

Bone is a frequent site of metastasis from cancers, as the bone microenvironment provides a rich bed of various hormones and cytokines for tumor growth (1). It is reported that transforming growth factor beta (TGF-β) and its associated pathway drive a vicious cycle for tumor growth and bone resorption (2). Bone consists of many types of cells, including hematopoietic and mesenchymal stem cells in bone marrow, as well as bone-forming osteoblasts, bone-resorbing osteoclasts, and osteocytes, the most abundant cell type in the bone matrix (3,4). Among bone marrow-derived cells of hematopoietic origin, T cells produce TGF-β and receptor activator of nuclear factor kappa B ligand (RANKL), which activate differentiation of macrophages to bone-resorbing osteoclasts (5). While the interactions of tumor cells with osteoclasts in the presence of TGF-β, RANKL, and interleukins have been extensively studied (6–8), interactions between tumor cells and osteocytes, which are thought to be a sensor for mechanotransduction (9), have not been fully explored.

In this study, we focused on two FDA-approved drugs, Fluphenazine (FP) and Trifluoperazine (TFP), and evaluated their roles in tumor-bone interactions. These two agents are modulators of dopaminergic signaling and currently used as antipsychotic medications (10,11). The dopamine system is involved in many neurological functions (12), but it is also important in other tissues, such as the cardiovascular and skeletal systems (13,14). Dopaminergic signaling is mediated via G protein-coupled dopamine receptors (D1, D2, D3, D4, and D5), and regulates voluntary movements and reward responses (15). This pathway is integral for many neural functions, and its deficiency causes neurological and psychiatric disorders such as Parkinson’s disease and schizophrenia (16). Dopaminergic signaling has recently been shown to be a potential target for preventing mammary tumor growth and bone metastasis using A77636, an agonist of DRD1 (17). Unlike FP and TFP, A77636 is not an FDA-approved drug. Furthermore, little is known about the effects of FP and TFP on tumor-bone interactions. In this study, we investigated their effects on mammary tumor cells, as well as bone-resorbing osteoclasts, bone-forming osteoblasts, and mechano-sensing osteocytes. Dopamine is reported to promote proliferation of bone-forming osteoblasts and mineralization of bone tissue (18).

To examine the efficacy of FP and TFP as well as interactions of mammary tumor cells with osteoclasts and osteocytes, we employed three dimensional (3D) spheroid cultures as well as monolayer cell cultures (19,20). Interactions of tumor cells with bone cells were examined by pre-mixing tumor and bone cells and forming a mosaic spheroid or fusing a pair of separately prepared spheroids consisting of tumor cells alone and bone cells alone. While we formed spheroids from 4T1.2 mammary tumor cells (21), RAW267.4 pre-osteoclast cells (22), MC3T3 osteoblast-like cells (23), and MLO-A5 osteocyte-like cells (24), our analysis of bone-tumor interactions was mostly focused on MLO-A5 cells in the presence and absence of FP and TFP. We used confocal microscopy to examine cellular morphology and viability of fluorescently labeled spheroids.

We hypothesized that FP and TFP suppress tumor growth and tumor-associated bone resorption via dopamine receptors. Since bone is one of the most frequent sites of metastasis

from breast cancer, interactions of tumor cells with the most abundant cells in bone matrix is our research aim. We further hypothesized that tumor-osteocyte interactions may favor immobilization of tumor cells in the bone microenvironment and restrain efficacy of DRD2 inhibitors. Dopamine receptors are members of the DRD1-like family (DRD1 and DRD5) or DRD2-like family (DRD2, DRD3, and DRD4). To evaluate the role of DRD1-like and DRD2-like receptors in the responses to FP and TFP, we employed siRNAs specific to these receptors. In bone-tumor interactions, we focused on the role of *Snail*, a transcription factor involved in the epithelial-to-mesenchymal transition (EMT) (25), ZO-1 (zonula occludens 1), as well as NFκB and AKT, two factors involved in tumor progression. ZO-1 is a tight junction-associated signaling protein, which mediates cell adhesion and is downregulated in EMT (26).

To evaluate direct and indirect tumor-bone interactions, we employed osteocyte-derived conditioned medium as well as a tumor-bone spheroid fusion assay. We examined the effects of secretory factors from osteocytes on tumor proliferation and tested the linkage of bone-tumor interactions to mesenchymal-to-epithelial transition (MET, a reversal of EMT) by determining and over-expressing *Snail* by plasmid transfection. Induction of MET at a potential site of metastasis for breast cancer cells has significant implications in regulating invasion and colonization of tumor cells in the bone microenvironment. These assays allowed us to evaluate the potential mechanism underlying bone-tumor interactions and their impact on the efficacy of FP and TFP. The results demonstrate that type I collagen and *Snail* play crucial roles in tumor-osteocyte interactions to enhance FP's and TFP's suppression of tumor migration and reduce their attenuation of tumor proliferation.

Materials and Methods

Cell culture

4T1.2 mouse mammary tumor cells (obtained from Dr. R. Anderson at Peter MacCallum Cancer Institute, Melbourne, Australia) were cultured in DMEM. RAW264.7 pre-osteoclast cells (ATCC TIB-71, Manassas, VA, USA), MC3T3 osteoblast-like cells (Sigma-Aldrich, St. Louis, MO, USA), and MLO-A5 osteocyte-like cells (obtained from Dr. L. Bonewald at Indiana University, IN, USA) were grown in αMEM. Mycoplasma testing was conducted using a Lonza mycoalert plus mycoplasma kit (Lonza Inc., Morristown, NJ, USA). For 4T1.2 cells, cell authentication testing was conducted using whole exome DNA sequencing (Agilent SureSelect Mouse Exon, Santa Clara, CA, USA). The culture media was supplemented with 10% fetal bovine serum and antibiotics, and cells were maintained at 37°C and 5% CO_2. Fluphenazine (FP; Sigma-Aldrich) and Trifluoperazine (TFP; Enzo Life Sciences, Farmingdale, NY, USA) were employed as modulators of dopaminergic signaling. Fluphenazine (438 Da) and Trifluoperazine (407 Da) are small synthetic agents used as antipsychotic medications in the treatment of schizophrenia. 4T1.2 cells were also treated with type I collagen (Corning, NY, USA). Cellular proliferation was examined using an MTT cell proliferation assay (Invitrogen, Carlsbad, CA, USA) with the procedure previously described (17).

Transfection of *Snail* plasmid and siRNA for dopamine receptors D1 and D2 (DRD1 and DRD2)

For overexpressing *Snail* protein, 4T1.2 tumor cells were transfected with a plasmid consisting of *Snail* coding sequence (SnailHA_pcDNA3; Addgene, Cambridge, MA, USA), while a blank plasmid vector (FLAG-HA-pcDNA3.1; Addgene) was used as a control. 4T1.2 cells were also treated with siRNA specific to *Drd1* (Life Technologies; siRNA: s65128) and *Drd2* (161556). As a nonspecific control, a negative siRNA (Silencer Select #1, Life Technologies) was used. Cells were transiently transfected with siRNA in Opti-MEM I medium with Lipofectamine RNAiMAX (Life Technologies). Twenty-four hours later, the medium was replaced by regular culture medium with reagents. The efficiency of silencing was assessed with immunoblotting 24 h after transfection.

Two-dimensional motility assay

A wound healing scratch motility assay was utilized to evaluate 2-dimensional cell motility (27). In brief, cells were grown on 12-well plates, and a plastic tip was used to scratch a gap onto the cell layer. After incubation, the areas newly occupied with cells in the scratched zone were imaged and measured with Image J (National Institutes of Health, Maryland, USA).

Osteoclast differentiation assay

Using RAW264.7 pre-osteoclast cells, an osteoclast differentiation assay was conducted in 96-well plates (28). During 6-day experiments growing cells in 20 ng/ml of RANKL, the culture medium was exchanged once on day 4. Adherent cells were fixed and stained with a tartrate resistant acid phosphate (TRAP)-staining kit (Sigma-Aldrich, Missouri, USA), according to the manufacturer's instructions. TRAP-positive multinucleated cells (> 3 nuclei) were identified as mature osteoclasts and counted.

Western blot analysis

Cells were lysed with a radio-immunoprecipitation assay buffer supplemented with protease inhibitors (Santa Cruz Biotechnology, Santa Cruz, CA, USA) and phosphatase inhibitors (Calbiochem, Billerica, MA, USA). Isolated proteins were fractionated using 10-15% SDS gels and electro-transferred to polyvinylidene difluoride membranes (Millipore, Billerica, MA, USA). We used antibodies against *Atf4*, p-*Akt*, *Akt*, caspase 3, cathepsin K, *eIF2*α, p-*eIF2*α, lamin B, *Lc3A/B II*, *Nfatc1*, *NFκB*, p-*NFκB*, *Snail*, *Zo-1* (Cell Signaling, Danvers, MA, USA), and β-actin (Sigma). Protein levels were assayed using a SuperSignal west femto maximum sensitivity substrate (Thermo Scientific, Waltham, MA, USA).

Formation and viability of 3D spheroids

Cells were cultured in Ultra-low attachment 96-well plates (S-BIO, New Hampshire, USA) at 1×10^4 cells/well for 4T1.2 cells, 2×10^4 cells/well for A5 cells, 2×10^4 cells/well for RAW cells. Cells were imaged every 24 h, and area and roughness were calculated with ImageJ. To observe spheroid formation of mixtures of cancer cells with osteocyte and osteoblast cells, IncuCyte ZOOM real-time imaging microscope was used to image cells every hour with fluorescent staining (Incucyte CytoLight Green and Red, Essen Bioscience, Michigan,

USA). In combination, 4T1.2, A5, and RAW cells were seeded at 1×10^4 cells/well, 3×10^3 cells/well, and 2×10^3 cells/well, respectively. A three-dimensional spheroid viability assay was conducted by plating 4T1.2, MLO-A5 and RAW 264.7 cells on ultra-low attachment 96-well plates at concentrations of 1×10^4, 2×10^4, and 2×10^4 cells/well, then incubated for 24 h. Treatment medium was exchanged, and spheroids were incubated for 72 h. The cell viability was measured with CellTiter-Glo® 3D Cell Viability Assay (Promega). To visualize 3D spheroid proliferation in response to medium exchange and drug treatment, a fluorescence-based cell proliferation kit was used (Click-iT™ EdU Alexa Fluor™ 488 Imaging Kit; Thermo-Fisher). After 24 h, cells were incubated with EdU for 3 h, then fixed and labeled, per manufacturer's instruction. Confocal microscope images were acquired with FV1000 (Olympus, Tokyo, Japan) and analyzed using ImageJ.

Animal models

The experimental procedures using animals were approved by the Indiana University Animal Care and Use Committee and were in compliance with the Guiding Principles in the Care and Use of Animals endorsed by the American Physiological Society. Mice were housed five per cage and provided with mouse chow and water *ad libitum*. In the mouse model of mammary tumor (29), 23 BALB/c female mice (~6 weeks, Harlan Laboratories) received subcutaneous injections of 4T1.2 cells (5.0×10^5 cells in 50 μl PBS) to the mammary fat pad on day 1. FP or TFP (1 mg/kg body weight) was administered subcutaneously into the area of cell injection every day, while the placebo animals received a vehicle control. The animals were sacrificed on day 18, and the weight of each tumor was measured. In the mouse model of bone metastasis (30), 33 BALB/c female mice received injection of 4T1.2 cells (1.0×10^5 cells in 50 μl PBS) to the right iliac artery. FP or TFP was administered daily via i.p. injection at 2 mg/kg body weight, and the animals were sacrificed on day 17. A whole body X-ray of each mouse was taken, and the tibia and femur were harvested for mechanical testing, μCT imaging, and histology. To examine the role of type I collagen in the bone microenvironment, 10 BALB/c female mice were employed, and type I collagen was co-injected with 4T1.2 cells (5×10^5 cells in 20 μl PBS with 50 μg/ml type I collagen) into the intra-tibial cavity.

μCT imaging

Micro-computed tomography was performed using Skyscan 1172 (Bruker-MicroCT, Kontich Belgium) (31). The harvested bone samples were wrapped in parafilm to maintain hydration and placed in a plastic tube and oriented vertically. Scans were performed at pixel size 8.99 μm. Using manufacturer-provided software, the images were reconstructed (nRecon v1.6.9.18) and analyzed (CTan v1.13).

Mechanical testing and histology

Mechanical testing was conducted using an ElectroForce loading device (TA Instruments, Eden Prairie, MN, USA). A sinusoidal force (1 N peak-to-peak force) was applied at 1 Hz, and the slope of force-displacement relationship was determined as tibial stiffness. For histology, bone samples were fixed in 10% neutral buffered formalin and decalcified in a 14% EDTA solution. They were then dehydrated through a series of graded alcohols, cleared

in xylene, and embedded in paraffin. H&E staining was conducted on the sagittal sections, and the distribution of tumor cells in the tibial bone cavity was determined.

Statistical analysis

The data were expressed as mean ± standard deviation. One-way analysis of variance was employed to examine statistical significance among groups, and Fisher's protected least significant difference was conducted *post hoc* to evaluate pairwise comparisons. Statistical significance for $p < 0.05$ was assumed.

Results

Inhibition of proliferation and differentiation of RAW264.7 pre-osteoclast cells

In order to evaluate the effects of FP and TFP on bone-resorbing osteoclasts, we conducted *in vitro* analysis using RAW264.7 pre-osteoclast cells. First, the relative proliferation of RAW264.7 cells using an MTT cell proliferation assay was significantly decreased by FP in a dose-dependent manner (Fig. 1A). Second, in response to RANKL-driven osteoclastogenesis, the phosphorylation level of eIF2α was elevated, and genes related to osteoclast function, such as NFATc1 and Cathepsin K, were downregulated by treatment with 1, 5, and 10 μM FP (Fig. 1B&C). The same trends were observed by TFP treatment (Fig. 1D-F). Third, the number of TRAP-positive, multi-nucleated cells induced by RANKL administration was decreased by FP and TFP (Fig. 1G&H). Lastly, 3D viability of RAW264.7 spheroids was significantly reduced by 10 and 20 μM TFP (Fig. 1I&J). Collectively, the result showed that FP and TFP inhibited proliferation and differentiation of RAW264.7 pre-osteoclast cells.

To evaluate the effects of FP and TFP on bone formation, we also examined bone-forming osteoblasts (MC3T3 osteoblast-like cells), as well as osteocytes (MLO-A5 osteocyte-like cells). Unlike their inhibitory effect to RAW264.7 cells, 5 μM FP and TFP did not significantly reduce proliferation of MC3T3 cells (Supplementary Fig. S1A). These agents elevated the protein levels of p-*eIF2*α and *Atf4*, a transcription factor important for bone formation (Supplementary Fig. S1B). Furthermore, they elevated osteoprotegerin (*Opg*) mRNA and osteocalcin (*Ocn*) mRNA (Supplementary Fig. S1C). *Opg* is an inhibitory factor of osteoclastogenesis, while *Ocn* is a marker for bone formation. The same trends in cell proliferation and protein expression were found in MLO-A5 cells (Supplementary Fig. S1D&E). In a 3D spheroid formation assay, the agents did not reduce spheroid size or luminescence-based survival of MC3T3 and MLO-A5 cells (Supplementary Fig. S1F&G).

Inhibitory effects on proliferation and migration of 4T1.2 mammary tumor cells

Thus far, the results with RAW264.7 cells, MC3T3 cells, and MLO-A5 cells support the action of these agents in protecting bone from resorption. Next, we examined their effects on 4T1.2 mammary tumor cells. First, the result from an MTT cell proliferation assay revealed that these agents inhibited proliferation of 4T1.2 cells (Fig. 2A). The levels of p-*eIF2*α, a marker for integrated stress, cleaved caspase, an apoptosis marker, and LC3A/B II, an autophagy marker, were elevated (Fig. 2B-D). Of note, the elevation of the autophagy marker indicates induction of a pro-survival pathway along with induction of apoptosis. A

2D motility assay showed that both agents reduced the healing of the scratched wound in a dose-dependent manner at 1, 5 and 10 μM (Fig. 2E, Supplementary Fig. S2A&B).

Next, FP and TFP action through dopamine receptors was examined. RNA interference using *Drd1* siRNA and *Drd2* siRNA, two dopamine receptor genes, revealed that partial silencing of *Drd2* significantly suppressed FP/TFP-induced inhibition of tumor proliferation and migration (Fig. 2F-H). Compared to the effect of *Drd2* siRNA, that of *Drd1* siRNA was less significant (Supplementary Fig. S2C-E). Using MDA-MB-231 breast cancer cells, we also confirmed that FP and TFP inhibited their proliferation (Supplementary Fig. S3A), elevated p-*eIF2α*, cleaved caspase 3, and LC3A/B II (Supplementary Fig. S3B), and decreased migration (Supplementary Fig. S3C). In MCF7 breast cancer cells, the same trends in proliferation (Supplementary Fig. S4A), protein expression (Supplementary Fig. S4B), and migration (Supplementary Fig. S4C) were observed. The result from the MTT cell proliferation assay was supported by an EdU cell proliferation assay, in which the relative proliferation rate of 4T1.2 cells, MDA-MB-231 cells, and MCF-7 cells was reduced by FP and TFP in a dose-dependent manner (Fig. 3A-C).

Expansion of the necrotic core in 4T1.2 spheroids by FP and TFP

We further examined the effects of these agents on tumor growth using 3D 4T1.2 tumor spheroids. We observed that the tumor spheroid developed a three-layered spherical structure composed of a necrotic core at the center, a quiescent shell around the necrotic core, and a proliferating zone on the surface (Fig. 3D). In response to 1, 5, and 10 μM FP and TFP, the necrotic core expanded along incubation time in a dose-dependent manner (Fig. 3D-F). Consistent with the expansion of the necrotic core, the luminescence level in the 3D viability assay was decreased by drug treatment (Fig. 3G), associated with an increased level of cleaved caspase 3 (Fig. 3H).

Suppression of tumor growth and bone loss in a mouse model

After examining the actions of FP and TFP on bone cells and tumor cells in monolayer cell cultures and in 3D spheroids, we conducted *in vivo* analysis using mouse models of mammary tumor and bone metastasis. First, 4T1.2 cells were inoculated to the mammary fat pad, and development of the mammary tumor was monitored (Fig. 4A-D). The results revealed that the size and weights of the tumors were significantly reduced by daily administration of FP or TFP. Second, we induced the migration of tumor cells into the right hind limb by injecting 4T1.2 cells into the right iliac artery. Using μCT images, we reconstructed the 3D structure of trabecular bone in the distal femur (Fig. 4E). Compared to placebo, FP- and TFP-treated samples presented a denser distribution of trabecular bone segments in the distal femur, with an increase in trabecular thickness (Fig. 4F). Compared to placebo, the bone volume was significantly higher in the FP-treated group but not in the TFP-treated group. In response to four-point bending mechanical test, the femur stiffness was greater in both FP- and TFP-treated groups (Fig. 4G).

Type I collagen is the most abundant protein in bone matrix. To evaluate the role of type I collagen in tumor growth and migration in the bone microenvironment, we co-injected type I collagen with 4T1.2 tumor cells into the left tibial cavity and conducted mechanical testing

and histological analysis. Mechanical testing revealed that compared to the contralateral tibia, tibial stiffness was significantly lowered after 2-3 weeks (Fig. 4H&I; Supplementary Fig. S5A). However, co-injection of collagen suppressed the reduction of stiffness. Histological analysis showed that co-injection of collagen facilitated scattering tumor cells throughout the tibial bone cavity by reducing their aggregation (Fig. 4J, Supplementary Fig. S5B).

Reduced Inhibitory Effects of FP and TFP by Interactions with RAW264.7 cells

The results so far indicate that the two agents in this study significantly alter the fate of tumor growth as well as bone remodeling. In order to understand the action of these agents in the bone microenvironment, we next examined interactions of 4T1.2 spheroids with RAW264.7 cells in the presence and absence of these agents. First, we evaluated indirect interactions using the conditioned medium isolated from RAW264.7 pre-osteoclast cells. RAW264.7 conditioned medium expanded the quiescent zone with an increase in live cells (Supplementary Fig. S6A). The 3D viability assay revealed that the conditioned medium elevated the number of live cells in the presence and absence of FP and TFP at 1 and 5 μM (Fig. 5A&B). In response to RAW264.7 pre-osteoclast-derived conditioned medium, expression of *Snail*, a transcription factor for inducing epithelial-to-mesenchymal transition (EMT), was upregulated (Fig. 5C). In a 3D co-culture, 4T1.2 cells did not mix with RAW264.7 cells, and they formed two separate spheroids (Supplementary Fig. S6B&C). In a spheroid fusion assay, 20 μM FP and TFP reduced the size of RAW264.7 spheroids.

Regulation of *Snail* and p-Akt by interactions with MLO-A5 cells

To further understand the interactions in the bone microenvironment, we examined 4T1.2 spheroids with osteocytes. Incubation of 4T1.2 spheroids with conditioned medium from MLO-A5 osteocyte cells showed a decrease in surface roughness and an increase in relative proliferation (Fig. 5D&E, Supplementary Fig. S6D). Confocal microscopy of 4T1.2 spheroids illustrated that, compared with control, MLO-A5-conditioned medium increased the number of Click-iT EdU-labeled dividing cells (Fig. 5E). Western blot analysis revealed that *Snail* was downregulated in 4T1.2 cells by MLO-A5-conditioned medium as well as FP and TFP (Fig. 5F-H). Of note, RAW264.7-conditioned medium elevated the protein level of *Snail* (Fig. 5C). However, the level of p-*Akt* was elevated by MLO-A5-conditioned medium and reduced by FP and TFP (Fig. 5F-H). The level of *Snail* was further reduced by simultaneous application of osteocyte-derived conditioned medium and FP/TFP (Fig. 5H). Unlike RAW264.7 cells, MLO-A5 cells freely mixed with 4T1.2 cells, and these two types of cells formed a single integrated spheroid (Fig. 5I). In the presence of MLO-A5 spheroid, the diameter of the 4T1.2 spheroid was slightly decreased, and administration of 20 μM FP and TFP further reduced the diameter (Fig. 5J).

Reduction in *Snail* by incubation with type I collagen

Osteocytes are surrounded by bone matrix, in which type I collagen is the most abundant protein. In response to MLO-A5-derived conditioned medium, downregulation of *Snail* and upregulation of *p-Akt* were sustained for 24 h (2, 3, 6, 12, and 24 h) (Fig. 6A). In order to evaluate the potential role of type I collagen in interactions of tumor spheroids with MLO-A5 osteocytes or their conditioned medium, we cultured 4T1.2 tumor spheroids in the

presence of type I collagen at 0.1 to 10 μg/ml (Fig. 6B) and measured their protein expression in 2D culture (Fig. 6C). Compared to tumor spheroids in the control medium, the medium with type I collagen made spheroids smaller and more circular with smoother surfaces (Fig. 6B, D&E). Associated with those phenotypic alterations, *Snail* protein was downregulated, and 4T1.2 cells became less migratory in a dose-dependent manner (Fig. 6C, F&G). Furthermore, the protein levels of *Zo-1*, p-*NFκB* and p-*Akt* were elevated (Fig. 6C). In the wound healing assay, motility of 4T1.2 cells was reduced by collagen, FP, and TFP, and the simultaneous application of collagen with FP/TFP further suppressed the migratory behavior of tumor cells (Fig. 6F&G).

Partial suppression of A5 medium effects by *Snail* overexpression

The results so far show that direct and indirect interactions of tumor cells with osteocytes shrink tumor spheroid size and alter expression of *Snail* and *Akt*. *Snail* is downregulated by FP and TFP as well as tumor-osteocyte interactions. We further evaluated the role of *Snail* using a wound healing assay, in which migratory behaviors of 4T1.2 cells were suppressed by MLO-A5 conditioned medium (Fig. 7A&B). When *Snail* plasmid was transfected into 4T1.2 cells to elevate its expression, *Zo-1* is downregulated (Fig. 7C), and the surface of the tumor spheroids became rougher, regardless of treatment with MLO-A5 conditioned medium or FP/TFP (Fig. 7D&E). Furthermore, compared to the vector control, *Snail* overexpression partially suppressed A5 medium-driven inhibition of cellular motility (Fig. 7F&G).

Discussion

This study presented that tumor-osteocyte interactions downregulated expression of *Snail* in 4T1.2 tumor cells and reduced the migratory behavior of 3D tumor spheroids. The interactions also elevated DNA replication in the proliferating surface of tumor spheroids by activating *NFκB* and *Akt* pathways. Compared to MLO-A5 osteocyte cells, RAW264.7 pre-osteoclast cells showed weaker affinity to tumor cells and *Snail* overexpression. Tumor-osteocyte interactions as well as type I collagen suppressed the inhibitory effect of FP and TFP on the proliferation of tumor cells, while they enhanced FP/TFP's suppression of tumor cell migration. Collectively, osteocytes appear to act as an attractant of tumor cells to the collagen-rich bone matrix, while osteoclasts act as a desensitizer of the action of FP and TFP on tumor cells in the 3D bone-like microenvironment. In the proposed mechanism (Fig. 7H), *Drd2* and osteocytes both suppress *Snail*, but they have opposing effects on tumor proliferation markers *Akt* and *NFκB*. Collagen-rich osteocytes promote tumor cell aggregation, while *Drd2* attenuates migratory tumor behavior.

FP is an antagonist of dopamine receptors D_1 and D_2, while TFP is an antagonist of D_2 dopamine receptor (32). TFP is also known to antagonize calmodulin (33). We have previously reported that A77636, a selective D_1 dopamine receptor agonist, prevents tumor growth and bone resorption (17). It is reported that the role of D_1 is opposite to that of D_2, and thus an agonist of D_1, like A77636, may exert the same effect of an antagonist of D_2, like FP and TFP. We have previously reported that A77636's action is in part mediated by the elevated phosphorylation of *eIF2α* (17). A77636 stimulated dopamine- and cAMP-

regulated phosphoprotein (DARPP32) that inhibits protein phosphate 1 and elevates the level of p-eIF2α. Furthermore, elevated p-eIF2α was shown to suppress tumor cell migration via inhibition of Rac1 and prevent bone resorption via suppression of NFATc1. Consistent with our previous study, we have also observed dose-dependent upregulation of p-*eIF2*α in 4T1.2 tumor cells and RAW264.7 pre-osteoclast cells by FP and TFP. In response to partial RNA silencing of *Drd1* and *Drd2*, the result indicated that FP/TFP-driven suppression of proliferation and migration of tumor cells was mainly mediated by *Drd2*.

In evaluating interactions of tumor cells to MLO-A5 cells and RAW264.7 cells, we employed 3D spheroid assays as well as monolayer cell cultures with conditioned media. Experiments with conditioned media allowed us to evaluate the effects of secretory factors, while spheroid co-culturing and fusion led to evaluation of direct interactions more relevant to the physiological microenvironment than monolayer cultures. In response to FP and TFP, the necrotic core of tumor spheroids was enlarged, and ATP availability on the proliferating surface was reduced in a 3D viability assay. Unlike RAW264.7 cells, which did not fuse well with 4T1.2 cells, MLO-A5 cells fused with 4T1.2 cells to merge completely. Conditioned medium from RAW264.7 cells spread tumor spheroids and expanded the proliferating zone on the spheroid surface. The conditioned medium from MLO-A5 cells, however, reduced surface roughness and slightly shrank the tumor spheroids. Although tumor spheroid size was reduced by fusion with MLO-A5, MLO-A5-conditioned medium elevated DNA replication of the proliferating zone of tumor spheroids. Taken together, MLO-A5 cells appeared to capture and nurture tumor cells.

To understand the mechanism of action in tumor-osteocyte interactions, we evaluated the role of type I collagen, the most abundant protein in bone matrix and rich in osteocyte-derived conditioned medium. We observed that type I collagen acted as an attractant and dwarfing agent of migratory tumor cells and converted them to less migratory, more proliferative cells. When collagen was heat-denatured, it lost its ability to attract migratory tumor cells. It is conceivable that interactions of type I collagen with tumor cells are mediated by integrins such as $\alpha_1\beta_1$, $\alpha_2\beta_1$, and $\alpha_{11}\beta_1$, and other bone matrix proteins may assist interactions via binding to collagens (34). Consistent with *in vitro* results, histological analysis showed that co-injection of type I collagen with tumor cells promoted the mixing and scattering of tumor cells, diffusing through the bone marrow cavity to form small but widely spread clusters. Collagen co-injection also reduced the weakening of bone stiffness measured by *in vivo* mechanical testing.

Incubation with type I collagen downregulated *Snail*, a transcription factor involved in EMT, and upregulated *Zo-1*, p-*Akt* and p-*NFκB*. *Snail* is regulated by various signals at the level of transcription as well as post-translation (35). *Zo-1* is associated with adhesion and tight junction linked cell-cell communication, while *Akt* and *NFκB* contribute to various mechanisms, including cellular proliferation. Bone matrix contains a variety of matrix proteins, and, in addition to type I collagen, the involvement of other proteins need to be evaluated. These results raise the possibility that matrix proteins, including type I collagen, may act as inducers of immobilization and proliferation of tumor cells in the bone microenvironment, which is commonly observed in MET (36), the reversal of EMT. Further

investigation of molecular and cellular behaviors of tumor cells is needed to understand the role of tumor-osteocyte interactions in MET.

Clinical reports on the usage of dopamine modulators on the risk of breast cancer vary. In ~140,000 cases of dopamine-deficient Parkinson's disease patients, administration of dopamine antagonist is shown to lower rates of breast cancer, even factoring in depression and suicide risk (37). In a separate study of ~53,000 cases, usage of dopamine antagonists increased the risk of breast cancer by 16% (38). In schizophrenia patients (~6,000 cases), results vary widely, ranging from 52% risk increase to 40% risk decrease (39). No clinical data are available for potential effects of FP and TFP on bone metastasis.

The results herein establish a link between bone cell secretions and tumor activity, though there are several limitations that should be noted. Dopamine receptor modulators FP and TFP and osteocyte-conditioned medium both reduced spheroid size and tumor migration, but they had opposing effects on cell proliferation. This study used mouse-derived cell lines of osteoblasts, osteoclasts, and osteocytes, as well as a triple-negative mammary tumor mouse cell line. Human cell lines as well as other breast cancer types should be used to translate these findings toward clinical relevance. Though these existing drugs are well-studied for use in psychiatric patients, their side effects must be carefully considered, or they might be selectively delivered to tumor cells. While FP and TFP were analyzed as antagonists to DRD2, these agents may have limited selectivity and interact with other DRDs.

Much previous work has shown the importance in osteoclast feedback with tumor cells in bone metastasis, but our work explores the role of osteocytes. This study demonstrates that tumor-osteocyte interactions decrease *Snail* expression and increase *Akt* and *NFκB* signaling in tumor cells, and those interactions alter the efficacy of dopamine-modulating FP and TFP. In the bone microenvironment, tumor-osteocyte interactions strengthen inhibition by FP and TFP on tumor migration but weaken their suppression of tumor proliferation. Furthermore, the result presents a mechanistic rationale for possible future research directions in using collagen-based or other osteocyte-derived secretory factors to capture or target metastatic tumor cells. Those factors might also be useful in disrupting the communication between osteocytes and metastatic tumor cells.

Supplementary Material

Refer to Web version on PubMed Central for supplementary material.

Acknowledgments

The authors appreciate Chie Deguchi and Rika Kondo for technical support.

Financial support: This study was in part supported by funds from 100 Voices of Hope (H. Nakshatri, H. Yokota) and NIH/NIAMS (NIH R01 AR052144 - H. Yokota).

References

1. Roodman GD. Mechanisms of bone metastasis. N Engl J Med [Internet]. 2004; 350:1655–64. Available from: http://www.ncbi.nlm.nih.gov/pubmed/15084698.

2. Gokulnath M, Swetha R, Thejaswini G, Shilpa P, Selvamurugan N. Transforming growth factor-β1 regulation of ATF-3, c-Jun and JunB proteins for activation of matrix metalloproteinase-13 gene in human breast cancer cells. Int J Biol Macromol [Internet]. 2017; 94:370–7. Available from: http://www.ncbi.nlm.nih.gov/pubmed/27751807.

3. Hadjidakis DJ, Androulakis II. Bone remodeling. Ann N Y Acad Sci [Internet]. 2006; 1092:385–96. [cited 2014 Jul 10]; Available from: http://www.ncbi.nlm.nih.gov/pubmed/17308163.

4. Bonewald LF. The amazing osteocyte. J Bone Miner Res [Internet]. 2011; 26:229–38. Available from: http://www.pubmedcentral.nih.gov/articlerender.fcgi?artid=3179345&tool=pmcentrez&rendertype=abstract.

5. Yasui T, Kadono Y, Nakamura M, Oshima Y, Matsumoto T, Masuda H, et al. Regulation of RANKL-induced osteoclastogenesis by TGF-β through molecular interaction between Smad3 and Traf6. J Bone Miner Res [Internet]. 2011; 26:1447–56. Available from: http://www.ncbi.nlm.nih.gov/pubmed/21305609.

6. Weilbaecher KN, Guise TA, McCauley LK. Cancer to bone: a fatal attraction. Nat Rev Cancer [Internet]. Nature Publishing Group. 2011; 11:411–25. Available from: http://www.ncbi.nlm.nih.gov/pubmed/21593787.

7. Chiechi A, Waning DL, Stayrook KR, Buijs JT, Guise TA, Mohammad KS. Role of TGF-β in breast cancer bone metastases. Adv Biosci Biotechnol [Internet]. 2013; 4:15–30. Available from: http://www.ncbi.nlm.nih.gov/pubmed/24558636.

8. Bendre MS, Montague DC, Peery T, Akel NS, Gaddy D, Suva LJ. Interleukin-8 stimulation of osteoclastogenesis and bone resorption is a mechanism for the increased osteolysis of metastatic bone disease. Bone [Internet]. 2003; 33:28–37. Available from: http://www.ncbi.nlm.nih.gov/pubmed/12919697.

9. Bonewald LF, Johnson ML. Osteocytes, mechanosensing and Wnt signaling. Bone [Internet]. 2008; 42:606–15. Available from: http://www.pubmedcentral.nih.gov/articlerender.fcgi?artid=2349095&tool=pmcentrez&rendertype=abstract.

10. Tardy M, , Dold M, , Engel RR, , Leucht S. Trifluoperazine versus low-potency first-generation antipsychotic drugs for schizophrenia; Cochrane database Syst Rev [Internet] 2014 CD009396Available from: http://www.ncbi.nlm.nih.gov/pubmed/25003310

11. Tardy M, , Huhn M, , Engel RR, , Leucht S. Fluphenazine versus low-potency first-generation antipsychotic drugs for schizophrenia; Cochrane database Syst Rev [Internet] 2014 CD009230Available from: http://www.ncbi.nlm.nih.gov/pubmed/25087165

12. Girault J-A, Greengard P. The neurobiology of dopamine signaling. Arch Neurol [Internet]. 2004; 61:641–4. Available from: http://www.ncbi.nlm.nih.gov/pubmed/15148138.

13. Tayebati SK, Lokhandwala MF, Amenta F. Dopamine and vascular dynamics control: present status and future perspectives. Curr Neurovasc Res [Internet]. 2011; 8:246–57. Available from: http://www.ncbi.nlm.nih.gov/pubmed/21722093.

14. Bliziotes M, Gunness M, Eshleman A, Wiren K. The role of dopamine and serotonin in regulating bone mass and strength: studies on dopamine and serotonin transporter null mice. J Musculoskelet Neuronal Interact. 2002; 2:291–5. [PubMed: 15758457]

15. Ott T, Jacob SN, Nieder A. Dopamine receptors differentially enhance rule coding in primate prefrontal cortex neurons. Neuron [Internet]. 2014; 84:1317–28. Available from: http://www.ncbi.nlm.nih.gov/pubmed/25482027.

16. Beaulieu J-M, Gainetdinov RR. The physiology, signaling, and pharmacology of dopamine receptors. Pharmacol Rev [Internet]. 2011; 63:182–217. Available from: http://www.ncbi.nlm.nih.gov/pubmed/21303898.

17. Minami K, Liu S, Liu Y, Chen A, Wan Q, Na S, et al. Inhibitory Effects of Dopamine Receptor D1 Agonist on Mammary Tumor and Bone Metastasis. Sci Rep [Internet]. 2017; 7:45686. Available from: http://www.ncbi.nlm.nih.gov/pubmed/28374823.

18. Lee DJ, Tseng HC, Wong SW, Wang Z, Deng M, Ko C-C. Dopaminergic effects on in vitro osteogenesis. Bone Res [Internet]. 2015; 3:15020. Available from: http://www.ncbi.nlm.nih.gov/pubmed/26558139.

19. Ho WY, Yeap SK, Ho CL, Rahim RA, Alitheen NB. Development of multicellular tumor spheroid (MCTS) culture from breast cancer cell and a high throughput screening method using the MTT

assay. PLoS One [Internet]. 2012; 7:e44640. Available from: http://www.ncbi.nlm.nih.gov/pubmed/22970274.

20. Chen A, Wang L, Li B-Y, Sherman J, Ryu JE, Hamamura K, et al. Reduction in Migratory Phenotype in a Metastasized Breast Cancer Cell Line via Downregulation of S100A4 and GRM3. Sci Rep [Internet] Springer US. 2017; 7:3459. Available from: http://www.ncbi.nlm.nih.gov/pubmed/28615627.
21. Bolin C, Tawara K, Sutherland C, Redshaw J, Aranda P, Moselhy J, et al. Oncostatin m promotes mammary tumor metastasis to bone and osteolytic bone degradation. Genes Cancer [Internet]. 2012; 3:117–30. Available from: http://www.ncbi.nlm.nih.gov/pubmed/23050044.
22. Raschke WC, Baird S, Ralph P, Nakoinz I. Functional macrophage cell lines transformed by Abelson leukemia virus. Cell. 1978; 15:261–7. [PubMed: 212198]
23. Wang D, Christensen K, Chawla K, Xiao G, Krebsbach PH, Franceschi RT. Isolation and characterization of MC3T3-E1 preosteoblast subclones with distinct in vitro and in vivo differentiation/mineralization potential. J Bone Miner Res [Internet]. 1999; 14:893–903. Available from: http://www.ncbi.nlm.nih.gov/pubmed/10352097.
24. Kato Y, Boskey A, Spevak L, Dallas M, Hori M, Bonewald LF. Establishment of an osteoid preosteocyte-like cell MLO-A5 that spontaneously mineralizes in culture. J Bone Miner Res [Internet]. 2001; 16:1622–33. Available from: http://www.ncbi.nlm.nih.gov/pubmed/11547831.
25. Wang Y, Shi J, Chai K, Ying X, Zhou BP. The Role of Snail in EMT and Tumorigenesis. Curr Cancer Drug Targets [Internet]. 2013; 13:963–72. Available from: http://www.ncbi.nlm.nih.gov/pubmed/24168186.
26. Lamouille S, Xu J, Derynck R. Molecular mechanisms of epithelial-mesenchymal transition. Nat Rev Mol Cell Biol [Internet]. 2014; 15:178–96. Available from: http://www.ncbi.nlm.nih.gov/pubmed/24556840.
27. Kamimura Y, Furukawa K, Kittaka D, Nishio M, Hamamura K, Fukumoto S, et al. Differential enhancing effects of alpha2,8-sialyltransferase on the cell proliferation and mobility. Int J Oncol [Internet]. 2005; 26:337–44. Available from: http://www.ncbi.nlm.nih.gov/pubmed/15645117.
28. Zhang J, Zhu L, Peng B. Effect of BioAggregate on osteoclast differentiation and inflammatory bone resorption in vivo. Int Endod J [Internet]. 2015; 48:1077–85. Available from: http://www.ncbi.nlm.nih.gov/pubmed/25358857.
29. Connolly EM, Harmey JH, O'Grady T, Foley D, Roche-Nagle G, Kay E, et al. Cyclo-oxygenase inhibition reduces tumour growth and metastasis in an orthotopic model of breast cancer. Br J Cancer [Internet]. 2002; 87:231–7. Available from: http://www.ncbi.nlm.nih.gov/pubmed/12107848.
30. Wang H, Yu C, Gao X, Welte T, Muscarella AM, Tian L, et al. The osteogenic niche promotes early-stage bone colonization of disseminated breast cancer cells. Cancer Cell [Internet]. 2015; 27:193–210. Available from: http://www.ncbi.nlm.nih.gov/pubmed/25600338.
31. Mabilleau G, Mieczkowska A, Libouban H, Simon Y, Audran M, Chappard D. Comparison between quantitative X-ray imaging, dual energy X-ray absorptiometry and microCT in the assessment of bone mineral density in disuse-induced bone loss. J Musculoskelet Neuronal Interact. 2015; 15:42–52. [PubMed: 25730651]
32. Seeman P. Atypical antipsychotics: mechanism of action. Can J Psychiatry [Internet]. 2002; 47:27–38. Available from: http://www.ncbi.nlm.nih.gov/pubmed/11873706.
33. Levin RM, Weiss B. Binding of trifluoperazine to the calcium-dependent activator of cyclic nucleotide phosphodiesterase. Mol Pharmacol. 1977; 13:690–7. [PubMed: 18661]
34. Sweeney SM, Orgel JP, Fertala A, McAuliffe JD, Turner KR, Di Lullo GA, et al. Candidate cell and matrix interaction domains on the collagen fibril, the predominant protein of vertebrates. J Biol Chem [Internet]. 2008; 283:21187–97. Available from: http://www.ncbi.nlm.nih.gov/pubmed/18487200.
35. Wu Y, Wang Y, Lin Y, Liu Y, Wang Y, Jia J, et al. Dub3 inhibition suppresses breast cancer invasion and metastasis by promoting Snail1 degradation. Nat Commun [Internet]. 2017; 8:14228. Available from: http://www.ncbi.nlm.nih.gov/pubmed/28198361.

36. Gunasinghe NPAD, Wells A, Thompson EW, Hugo HJ. Mesenchymal-epithelial transition (MET) as a mechanism for metastatic colonisation in breast cancer. Cancer Metastasis Rev [Internet]. 2012; 31:469–78. Available from: http://www.ncbi.nlm.nih.gov/pubmed/22729277.

37. Lalonde FM, Myslobodsky M. Are dopamine antagonists a risk factor for breast cancer? An answer from Parkinson's disease. Breast [Internet]. 2003; 12:280–2. Available from: http://www.ncbi.nlm.nih.gov/pubmed/14659314.

38. Wang PS, Walker AM, Tsuang MT, Orav EJ, Glynn RJ, Levin R, et al. Dopamine antagonists and the development of breast cancer. Arch Gen Psychiatry [Internet]. 2002; 59:1147–54. Available from: http://www.ncbi.nlm.nih.gov/pubmed/12470131.

39. Bushe CJ, Bradley AJ, Wildgust HJ, Hodgson RE. Schizophrenia and breast cancer incidence: a systematic review of clinical studies. Schizophr Res [Internet]. 2009; 114:6–16. Available from: http://www.ncbi.nlm.nih.gov/pubmed/19695837.

Significance

Findings provide novel insight into the cellular cross talk in the bone microevironment and the effects of dopamine modulators on mammary tumor cells and osteocytes.

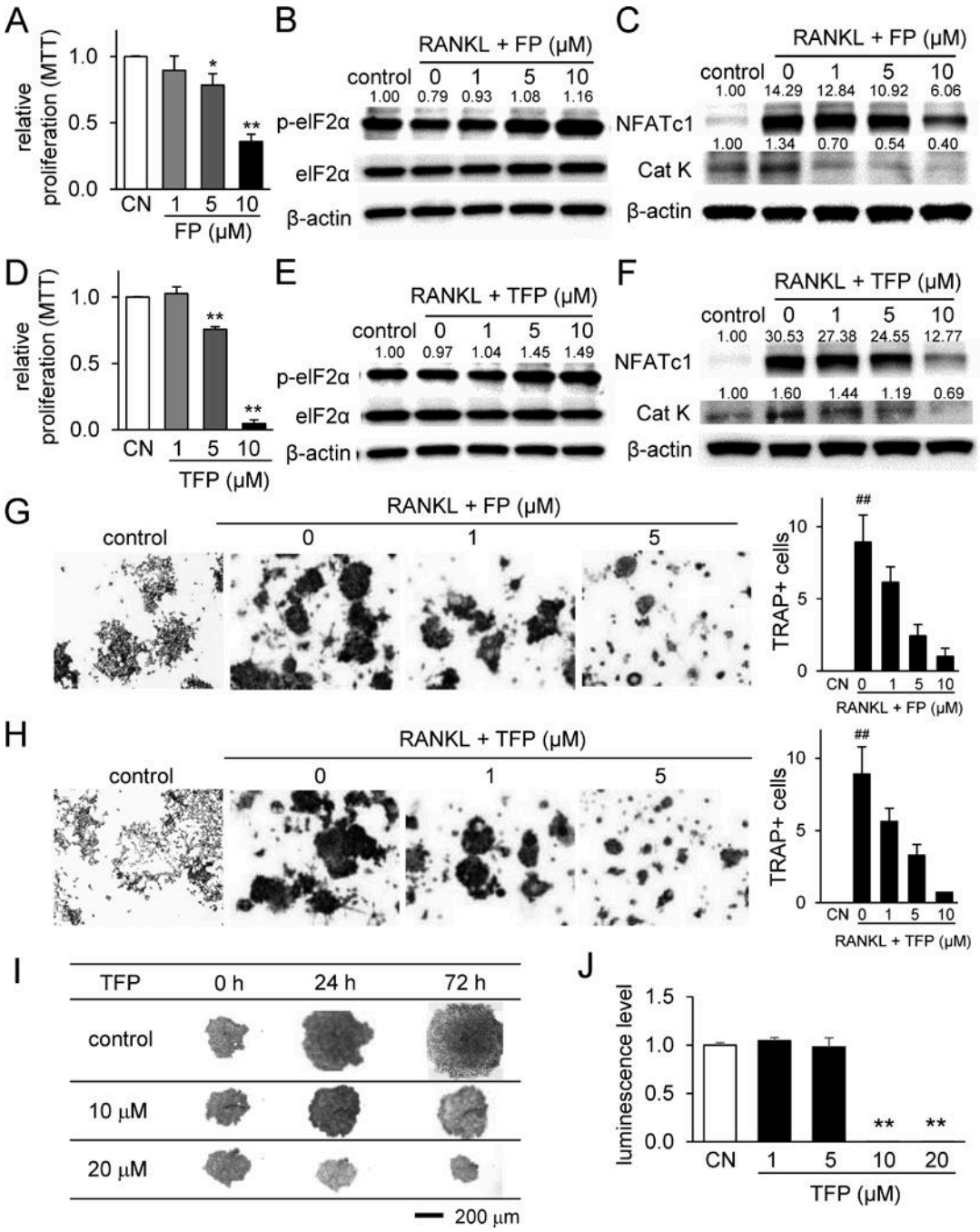

Figure 1.

Inhibition of proliferation and differentiation of RAW264.7 pre-osteoclast cells by Fluphenazine and Trifluoperazine. Of note, CN = control, FP = Fluphenazine, and TFP = Trifluoperazine. The single and double asterisks indicate $p < 0.05$ and $p < 0.01$, respectively, and the double hashtag marks $p < 0.01$ to the control in the absence of RANKL. (A&B) Reduction in cellular proliferation, and upregulation of p-*eIF2*α by Fluphenazine. (C) Downregulation of *NFATc1* and Cathepsin K by Fluphenazine. (D&E) Reduction in cellular proliferation, and upregulation of p-*eIF2*α by Trifluoperazine. (F) Downregulation of

NFATc1 and Cathepsin K by Trifluoperazine. (G&H) Suppression of RANKL-driven osteoclastogenesis by Fluphenazine and Trifluoperazine, respectively. (I&J) Dose-dependent inhibition of cellular proliferation in 3D spheroids and a decrease in 3D cell viability by Trifluoperazine.

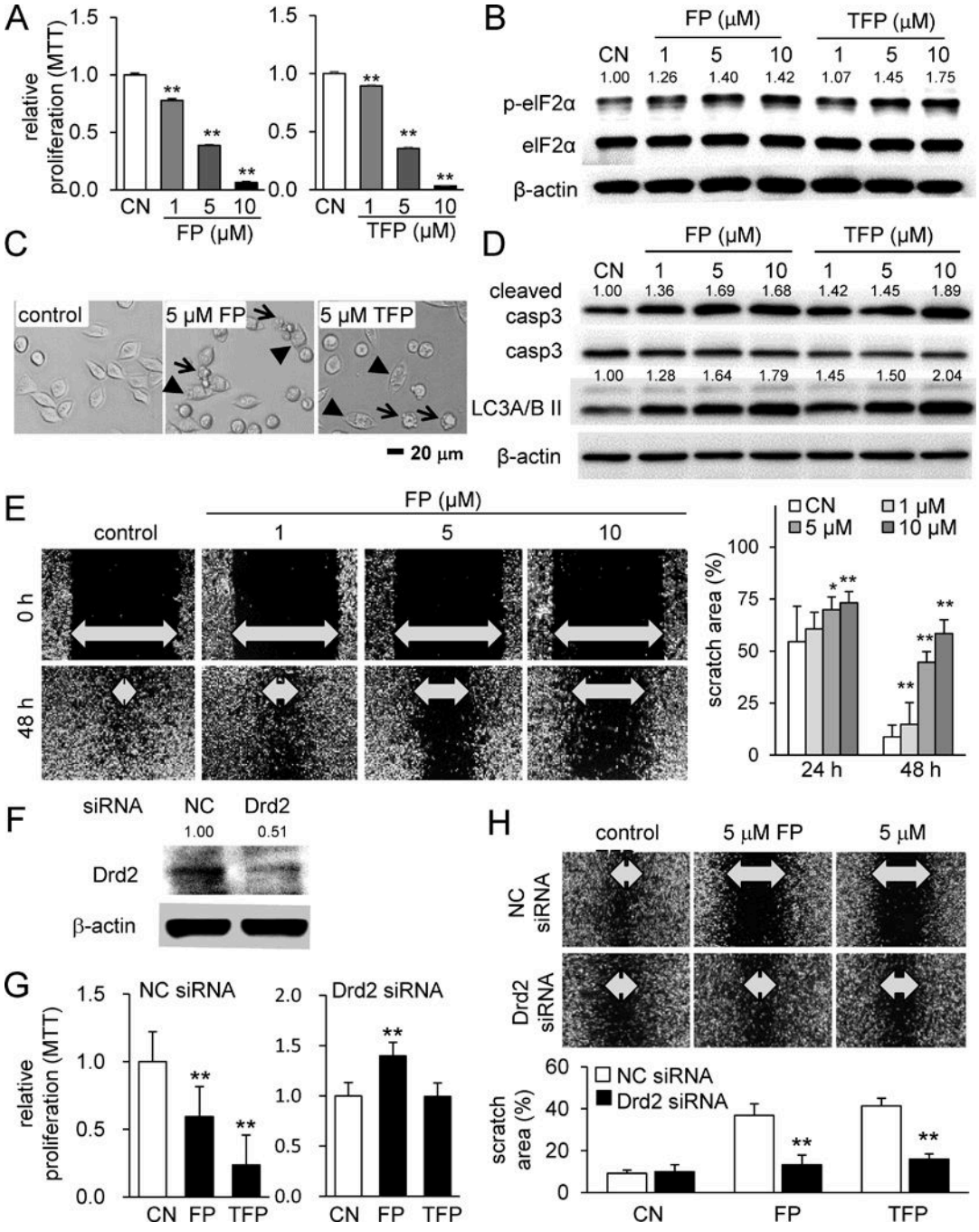

Figure 2.

Inhibitory effects of Fluphenazine and Trifluoperazine on proliferation and migration of 4T1.2 mammary tumor cells. Of note, CN = control, FP = Fluphenazine, and TFP = Trifluoperazine. The single and double asterisks indicate $p < 0.05$ and $p < 0.01$, respectively. (A) Reduced proliferation of 4T1.2 cells in response to Fluphenazine or Trifluoperazine. (B) Elevation of p-*eIF2α* by Fluphenazine and Trifluoperazine. (C) Representative cell images in response to 5 μM Fluphenazine or Trifluoperazine. The arrow indicates apoptotic cells, while the arrow head marks autophagic cells. (D) Elevation of the cleaved caspase 3 (marker

for apoptosis) and *Lc3A/B II* (marker for autophagy) in response to Fluphenazine or Trifluoperazine. (E) Retarded migration of 4T1.2 cells by 1, 5 or 10 μM Fluphenazine in a dose dependent manner. (F-H) Suppression of the inhibitory effect of Fluphenazine and Trifluoperazine on proliferation and migration by RNA silencing with *Drd2* siRNA.

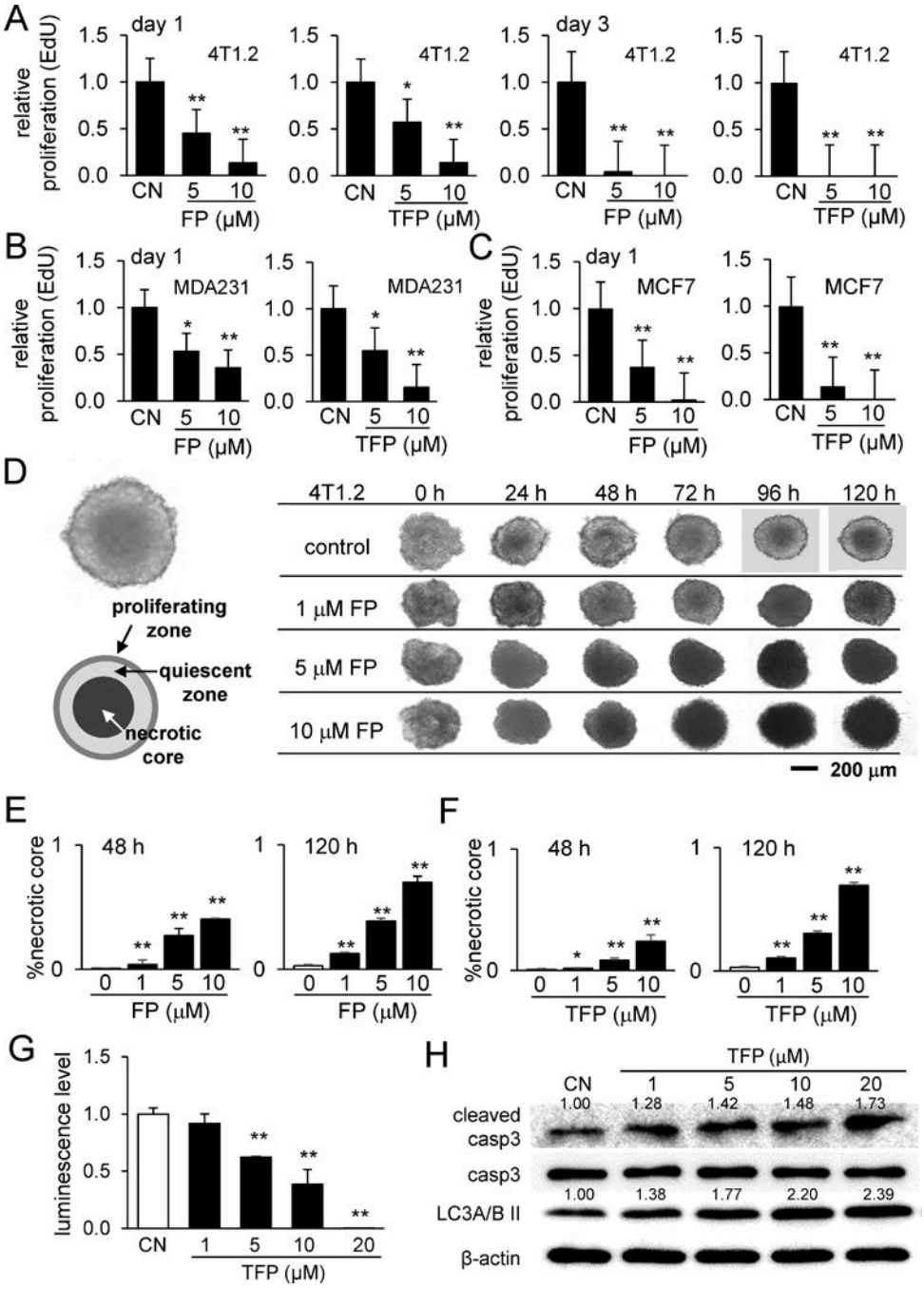

Figure 3.

Responses of tumor cells (4T1.2 cells, MDA-MB-231 cells, and MCF7 cells) to Fluphenazine and Trifluoperazine. Of note, CN = control, FP = Fluphenazine, and TFP = Trifluoperazine. The single and double asterisks indicate $p < 0.05$ and $p < 0.01$, respectively. (A-C) EdU-based relative proliferation of 4T1.2 cells, MDA-MB-231 cells, and MCF cells, respectively. (D) Temporal alterations in morphology of 4T1.2 spheroids in response to 1, 5, and 10 μM Fluphenazine in 24, 48, 72, 94, and 120 h. (E&F) Increased relative area of the necrotic core by Fluphenazine and Trifluoperazine, respectively. (G) Decrease in 3D cell

viability by 10 and 20 μM Trifluoperazine. (H) Elevation of the cleaved caspase 3 (marker for apoptosis) and *Lc3A/B II* (marker for autophagy) in response to Trifluoperazine.

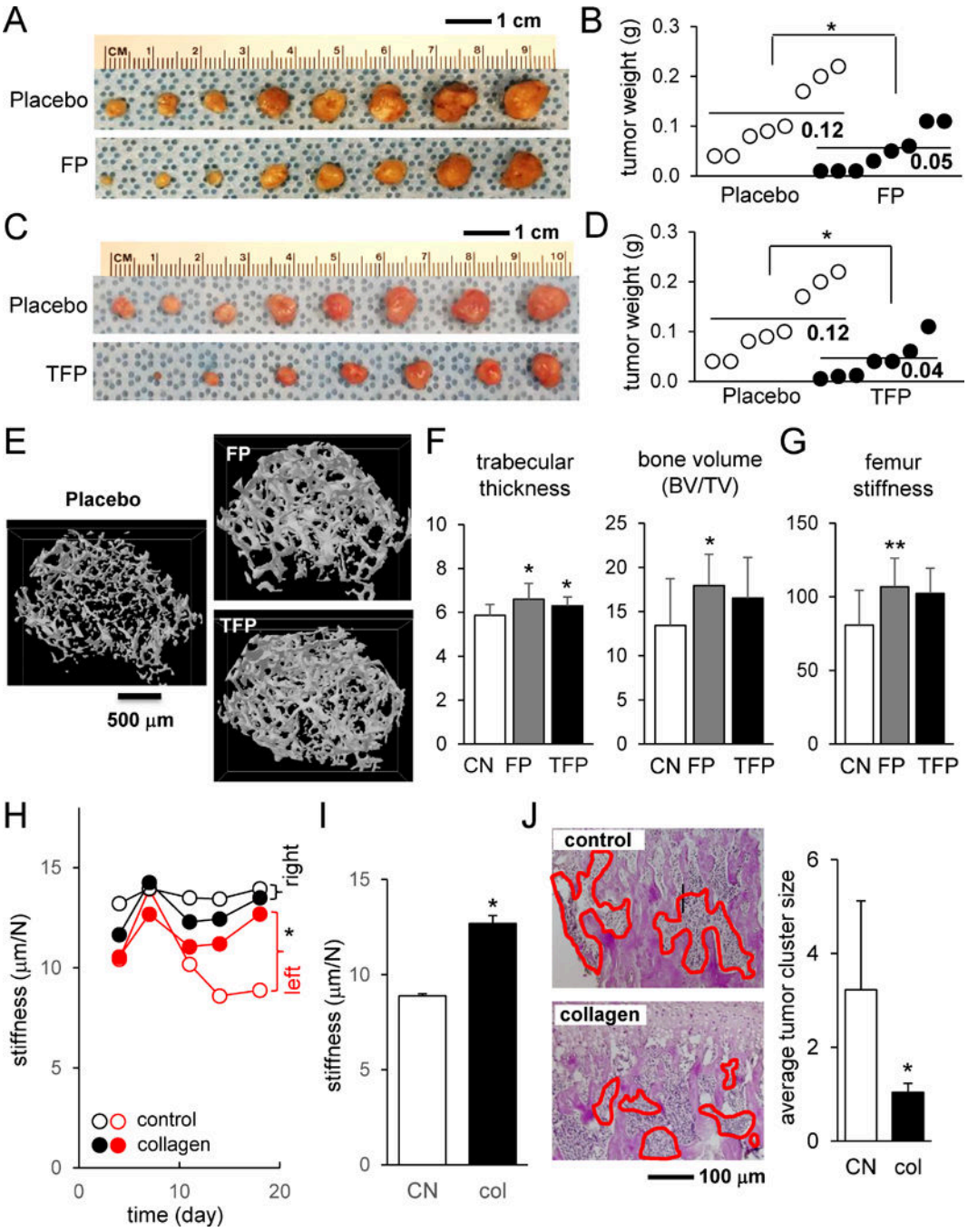

Figure 4.

Effects of Fluphenazine, Trifluoperazine, and collagen in a mouse model of mammary tumor and bone metastasis. Of note, FP = Fluphenazine, and TFP = Trifluoperazine. The single asterisk indicates $p < 0.05$. (A&B) Suppression of tumor growth at the mammary pad by Fluphenazine. (C&D) Suppression of tumor growth at the mammary pad by Trifluoperazine. (E) Reconstructed 3D μCT images of the distal femur for the placebo, Fluphenazine-treated, and Trifluoperazine-treated samples. (F) Trabecular thickness and bone volume. (G) Femur stiffness in four-point bending mechanical test. (H&I) Suppression of reduction in bone

stiffness by co-injection of collagen into the tibia. (J) Scattered distribution of 4T1.2 tumor cells (highlighted in red) in the tibial bone cavity and smaller average tumor cluster size by co-injection of collagen.

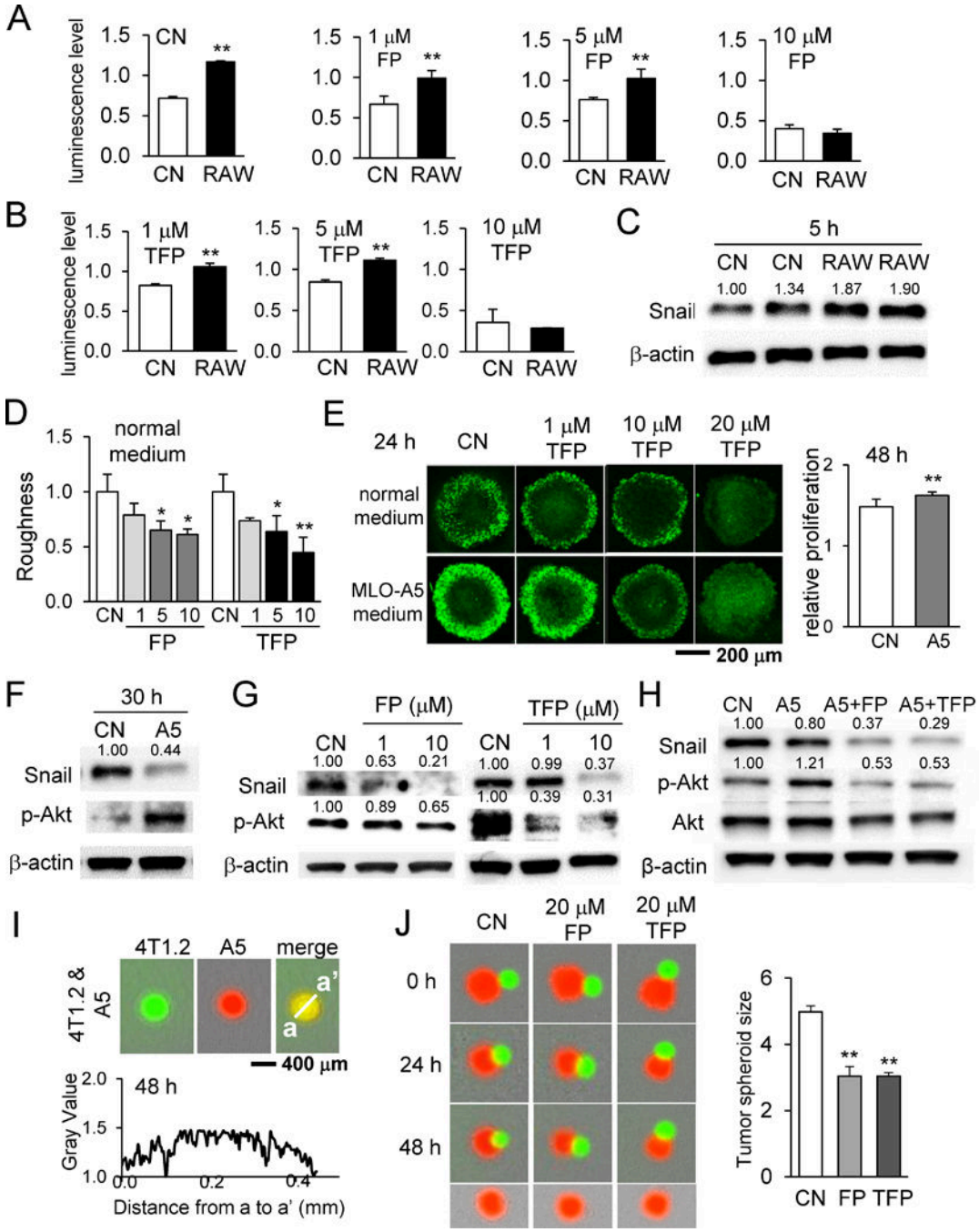

Figure 5.

Effects of RAW264.7 osteoclast-conditioned medium and MLO-A5 osteocyte-conditioned medium on 4T1.2 spheroids in the presence and absence of Fluphenazine or Trifluoperazine. Of note, CN = control, FP = Fluphenazine, and TFP = Trifluoperazine. The single and double asterisks indicate $p < 0.05$ and $p < 0.01$, respectively. (A&B) Alteration in 3D cell viability of 4T1.2 spheroids by the conditioned medium from RAW264.7 cells. (C) Upregulation of *Snail* protein by RAW264.7 conditioned medium. (D) Roughness of 4T1.2 spheroids in response to Fluphenazine or Trifluoperazine. (E) 3D cell viability and relative

proliferation of 4T1.2 spheroids in response to Fluphenazine or Trifluoperazine. (F-H) Alterations in *Snail* and p-*Akt* in response to MLO-A5 conditioned medium, Fluphenazine, and/or Trifluoperazine. (I) Interactions of 4T1.2 cells (green) and MLO-A5 cells (red). These two types of cells completely mixed. (J) Shrinkage of 4T1.2 spheroids (red) by 20 μM Fluphenazine or Trifluoperazine in the presence of MLO-A5 spheroids (green). The size of 4T1.2 spheroids (red) was significantly reduced by Fluphenazine or Trifluoperazine.

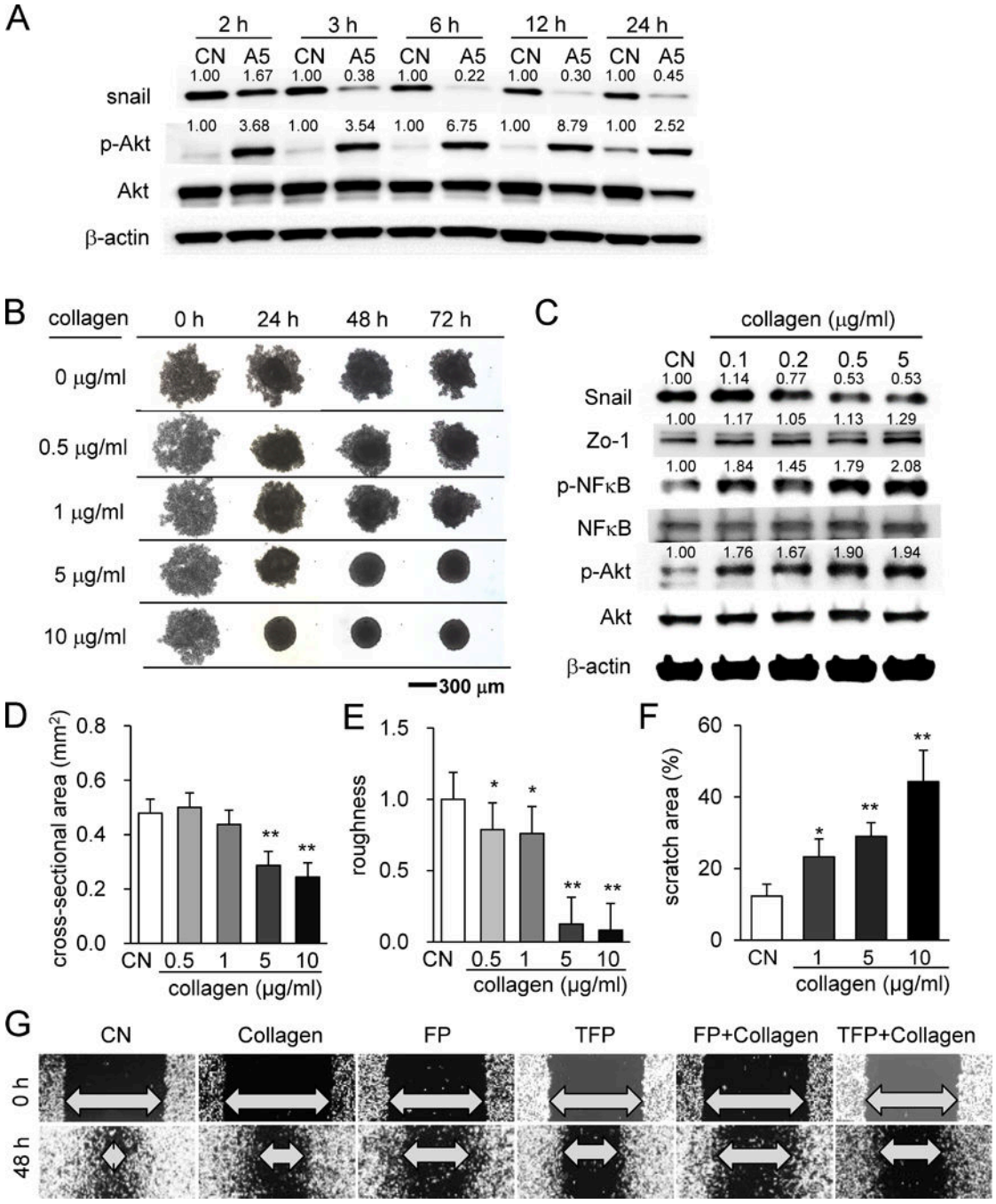

Figure 6.

Effect of collagen on tumor spheroids and cellular motility. (A) Effects of MLO-A5-derived conditioned medium on expression of *Snail*, p-*NFκB*, and p-*Akt*. (B) 4T1.2 tumor spheroids in response to collagen in the medium. (C) Effects of collagen on expression of *Snail*, p-*NFκB*, and p-*Akt*. (D&E) Effects of collagen on spheroid cross-sectional area and surface roughness. (F&G) Reduction in cellular motility of 4T1.2 cells by type I collagen and/or FP/TFP.

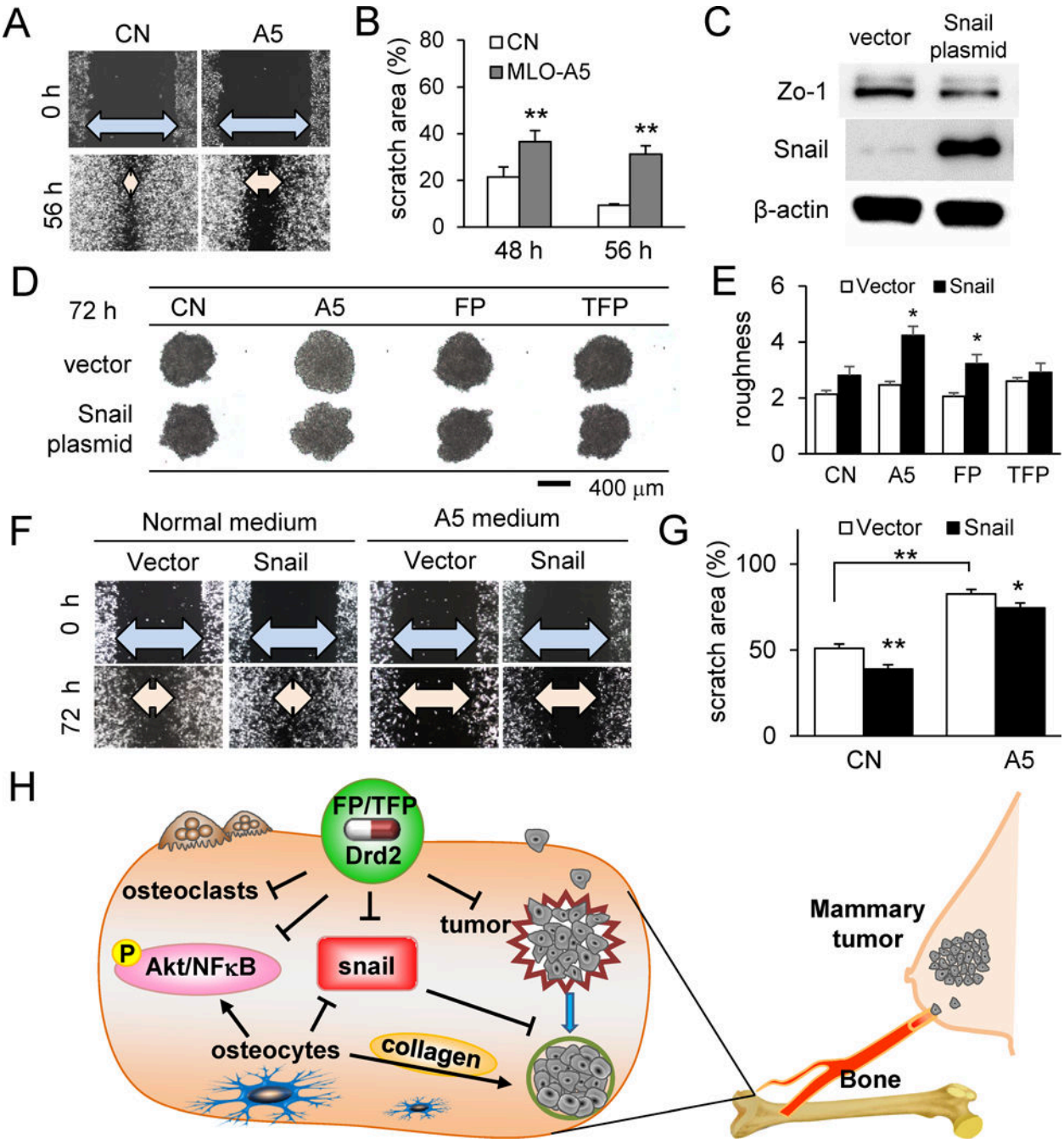

Figure 7.

Effects of upregulated *Snail* expression in 4T1.2 cells. Of note, CN = control, A5 = MLO-A5 osteocyte-like cells, FP = Fluphenazine, and TFP = Trifluoperazine. The single and double asterisks indicate $p < 0.05$ and $p < 0.01$, respectively. (A&B) Retarded migration of 4T1.2 cells by MLO-A5 conditioned medium. (C) Upregulation of *Snail* expression by transfection of *Snail* plasmid. (D&E) Effects of transfection of *Snail* plasmid on surface roughness. (F&G) Partial suppression of A5-conditioned medium driven reduction in migration by transfection of *Snail* plasmid. (H) Proposed mechanism of tumor-osteocyte

interactions with *Drd2* inhibitors. FP and TFP, inhibitors of *Drd2*, reduce Snail expression, osteoclast activity, *Akt* and *NFκB* proliferation markers, and tumor cell migration. Osteocyte interaction reduces Snail expression and cell migration, but increases *Akt* and *NFκB* expression.